

Experimental studies of the NaK $1^3\Delta$ state

J. Huennekens,^{a)} I. Prodan,^{b)} A. Marks, L. Sibbach,^{c)}
E. Galle,^{d)} and T. Morgus

Department of Physics, 16 Memorial Dr. East, Lehigh University, Bethlehem, Pennsylvania 18015

Li Li

Department of Physics, Tsinghua University, Beijing 100084, China

(Received 26 May 2000; accepted 26 July 2000)

The NaK $1^3\Delta$ state has been studied by the perturbation-facilitated optical–optical double resonance technique. Mixed singlet–triplet levels, $A(2)^1\Sigma^+(v_A, J) \sim b(1)^3\Pi(v_b, J)$, were pumped from thermally populated rovibrational levels of the ground state, $X(1)^1\Sigma^+(v_X, J \pm 1)$, using a single-mode cw dye laser. A single-mode cw Ti:Sapphire laser was then used to further excite the NaK molecules to various $1^3\Delta(v_\Delta, N_\Delta, J_\Delta)$ rovibrational levels which were detected by observing collision-induced $^3\Lambda \rightarrow a(1)^3\Sigma^+$ fluorescence in the green part of the spectrum. The measured energies of the $1^3\Delta(v_\Delta, N_\Delta)$ levels were fit to a Dunham expansion, and the Dunham coefficients were used to construct the RKR potential curve. Absolute numbering of the $1^3\Delta$ state vibrational levels was established by a comparison of experimental and calculated $1^3\Delta(v_\Delta, N_\Delta, J_\Delta) \leftarrow b(1)^3\Pi(v_b, J_b)$ absorption line strengths. A deperturbation program was used to determine the vibration-dependent $1^3\Delta$ state spin–orbit interaction parameter. Hyperfine structure of the $1^3\Delta$ state was studied, and the Fermi-contact interaction term for this state was determined to be $\sim 0.0111 \text{ cm}^{-1}$. © 2000 American Institute of Physics. [S0021-9606(00)00140-9]

I. INTRODUCTION

Over the last two decades, the optical–optical double resonance (OODR) technique has been used to obtain vast amounts of data concerning many electronic states of alkali diatomic molecules.^{1–42} When combined with narrow band continuous wave (cw) lasers, this technique is inherently Doppler-free, so that very high resolution excitation spectra can be obtained. Most previous work has concentrated on the homonuclear diatomics Li_2 ,^{1–9} Na_2 ,^{10–19} and K_2 .^{20–27} However, several groups have also used OODR to study high lying electronic states of NaK^{28–38} and other^{39–42} heteronuclear alkali molecules. In most cases, the goal has been to obtain spectroscopic constants of the electronic states and map the electronic potential as a function of internuclear distance. Relative intensities have been used to map transition dipole moments as functions of internuclear separation,^{36,43,44} and line shapes have been used to investigate predissociation,^{6,31–33,45–47} tunneling through barriers,^{8,17,28,29} and collisional quenching.^{31,48} Studies of collision-induced satellite lines have been used to investigate electronic, vibrational, and rotational energy transfer.^{2,6,7,23,38,47,49–52}

Due to the dipole selection rule on spin, $\Delta S = 0$, and the fact that the electronic ground state of all alkali molecules is a spin singlet ($S = 0$), most previous OODR work has in-

involved studies of high-lying singlet electronic states. However, perturbations can couple specific rovibrational levels of some singlet and triplet electronic states, most notably the $b^3\Pi$ and $A^1\Sigma^+$ states. These perturbed or mixed levels act as “windows” into the triplet manifold. This allows alkali diatomic triplet electronic states to be studied by a variant of the OODR technique called “perturbation-facilitated optical–optical double resonance” (PFOODR).^{43–47,53–75}

Alkali triplet states typically exhibit pronounced hyperfine structure due to the interaction between the electron spin and nuclear spin magnetic dipole moments. The Doppler-free nature of the cw PFOODR technique has allowed the study of the hyperfine structure of many triplet electronic states of Na_2 ,^{47,62–67,76–79} and similar studies have also been carried out for a few states of Li_2 ,^{47,54,55} and NaRb .^{40,80} The hyperfine structure of the NaK $c(2)^3\Sigma^+$ state has been studied in molecular beams^{81–83} and with a polarization spectroscopy variant of the PFOODR technique.^{44,73} The latter technique has also been used to study the hyperfine structure of the lowest NaK triplet state $a(1)^3\Sigma^+$.^{74,75}

In the present work we report PFOODR studies of the NaK $1^3\Delta$ state, which dissociates to the atomic limit $\text{Na}(3S_{1/2}) + \text{K}(3D_{5/2})$. A total of 771 $1^3\Delta(v, N, J, e/f)$ levels with $3 \leq v \leq 36$ were excited from four sets of $A(2)^1\Sigma^+ \sim b(1)^3\Pi_{\Omega=0}$ window levels. The $1^3\Delta$ state is intermediate between the Hund’s case a and case b coupling schemes, but much closer to case b. This results in a unique rotational line pattern that allows these transitions to be easily identified. We analyzed the level energies as a function of v and N to determine a set of Dunham coefficients. The latter was then used to determine the RKR potential curve for the $1^3\Delta$ state, which was compared to recent calculations of Magnier and

^{a)} Author to whom correspondence should be addressed.

^{b)} Present address: Department of Physics, Rice University, MS-61, P.O. Box 1892, Houston, Texas 77005-1892.

^{c)} Present address: Department of Physics and Earth Science, Moravian College, Bethlehem, Pennsylvania 18018.

^{d)} Present address: Department of Physics, Middlebury College, Middlebury, Vermont 05753.

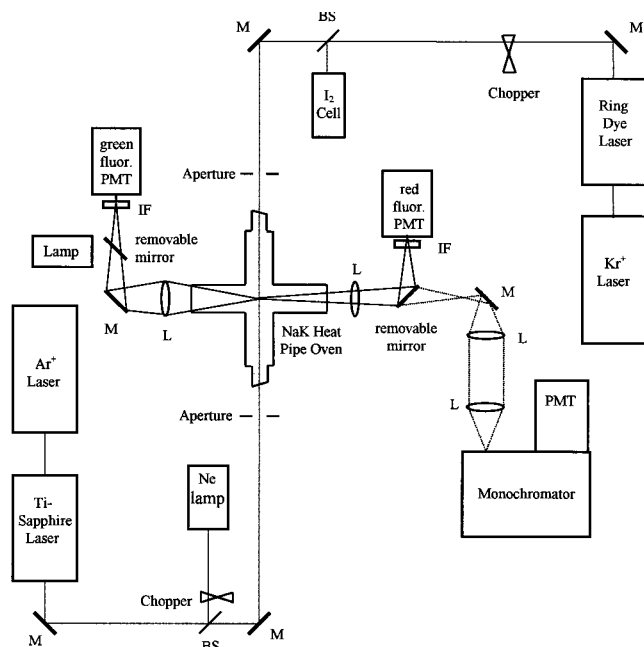


FIG. 1. Experimental setup. L, M, and BS represent lens, mirror, and beam-splitter, respectively, while IF and PMT refer to interference filter and photomultiplier tube, respectively.

Millié.⁸⁴ A deperturbation program LSQ⁸⁵ was then used to determine the $1^3\Delta$ state spin-orbit constant. The hyperfine structure of the $1^3\Delta$ state was also well resolved, and we analyzed this structure to obtain a value for the Fermi contact constant.

This paper is organized as follows. In Sec. II we describe the experimental setup. Analysis of the rotational level structure is described in Sec. III A, and the Dunham coefficients and RKR potential determined from the data are presented in Sec. III B. In Sec. III C we describe the calculation of excitation line intensities that were used to establish the absolute vibrational numbering of the $1^3\Delta$ state. The deperturbation analysis resulting in the determination of the spin-orbit constant is presented in Sec. III D, and the analysis of the $1^3\Delta$ state hyperfine structure is described in Sec. III E. Brief mention of the collisional “gateway” effect is made in Sec. III F. Finally, our conclusions are presented in Sec. IV.

II. THE EXPERIMENT

The experimental setup is shown in Fig. 1 and is similar to that used in Ref. 36. The sodium-potassium mixture was contained in a four-arm cross heat-pipe oven,⁸⁶ which was heated to $T \sim 365\text{--}395^\circ\text{C}$ in the central region to vaporize the metal. Argon buffer gas (pressure $\sim 0.5\text{--}1.5$ Torr) was used to keep the alkali metal away from the windows, which were maintained at room temperature using water cooling.

A Coherent model 699-29 single-mode cw dye laser, pumped by a 5 W krypton ion laser, produced $\sim 240\text{--}490$ mW power in the 730–775 nm range using LD700 dye. This dye laser (the PUMP laser) was tuned to specific $b(1)^3\Pi(v_b, J) \sim A(2)^1\Sigma^+(v_A, J) \leftarrow X(1)^1\Sigma^+(v_X=0, J \pm 1)$ transitions of the NaK molecule. A Coherent model 899-29 single-mode cw Ti:Sapphire laser, pumped by a 10 W argon

ion laser, produced 100–600 mW of power in the range 730–920 nm using short-wavelength and mid-wavelength optics. This Ti:Sapphire laser (the PROBE) was used to further excite the NaK molecules, from the $b(1)^3\Pi(v_b, J) \sim A(2)^1\Sigma^+(v_A, J)$ window levels populated by the PUMP laser, to various $1^3\Delta(v_\Delta, N_\Delta, J_\Delta)$ levels with $J_\Delta = J - 1, J, J + 1$. The two counterpropagating lasers were gently focused using 1.0 and 1.5 m focal length lenses for the PUMP and PROBE laser, respectively, and carefully overlapped at the center of the oven.

Fluorescence was observed using three detectors shown in Fig. 1. A freestanding photomultiplier tube (Hamamatsu R406, “red fluorescence PMT” in Fig. 1), equipped with a 700–1000 nm bandpass filter, was used to monitor total $A(2)^1\Sigma^+(v_A, J) \rightarrow X(1)^1\Sigma^+(v_X, J \pm 1)$ fluorescence at right angles to the laser propagation direction. This fluorescence signal was used to tune the PUMP laser onto line center of a particular $b(1)^3\Pi(v_b, J) \sim A(2)^1\Sigma^+(v_A, J) \leftarrow X(1)^1\Sigma^+(v_X, J \pm 1)$ transition, after which the PUMP laser frequency was fixed. The PROBE laser was then scanned, and excitation from the mixed level $b(1)^3\Pi(v_b, J) \sim A(2)^1\Sigma^+(v_A, J)$ into the $1^3\Delta$ state was monitored by detecting collision-induced $^3\Lambda \rightarrow a(1)^3\Sigma^+$ fluorescence in the green part of the spectrum (480–510 nm) with a second freestanding PMT (Hamamatsu R928, “green fluorescence PMT” in Fig. 1). This detector was equipped with a set of three 364–539 nm bandpass filters (Oriel model 51710) with a 465 nm transmission peak. Transitions to levels of the $1^3\Delta$ state could easily be detected in these Doppler-free excitation spectra by their characteristic signature (see Sec. III A). The PUMP laser was chopped and lock-in detection employed. Removal of an indexer-mounted mirror from the “red” fluorescence path allowed resolved fluorescence to be recorded using a monochromator/PMT system. In this case, the frequencies of both lasers were fixed to a specific double-resonance transition, either laser could be chopped, and the monochromator grating was scanned.

The wave meter of the PUMP laser was calibrated by comparing frequencies of I_2 laser-induced fluorescence signals with those listed in the iodine atlas.⁸⁷ The PROBE laser wave meter was calibrated using optogalvanic signals from neon transitions in a hollow cathode lamp. Energies of $1^3\Delta(v, N, J)$ levels obtained in this manner are considered accurate to $\sim 0.02\text{ cm}^{-1}$.

III. ANALYSIS AND RESULTS

A. Rotational level structure

Nearly degenerate levels of the $A(2)^1\Sigma^+(v_A, J)$ and $b(1)^3\Pi_{\Omega=0}(v_b, J)$ states, with the same rotational quantum number J , are coupled together by the spin-orbit interaction. The interaction results in true eigenstates that are mixtures of the unperturbed singlet and triplet wave functions. These singlet-triplet mixed levels $A(2)^1\Sigma^+(v_A, J) \sim b(1)^3\Pi_{\Omega=0}(v_b, J)$ act as “window levels,” allowing access into higher triplet states.

The locations of window levels can be predicted by plotting the energies of the $A(2)^1\Sigma^+(v_A, J)$ and $b(1)^3\Pi_{\Omega=0}(v_b, J)$ rotational levels, calculated using the ac-

curate $A(2)^1\Sigma^+(v_A, J)$ and $b(1)^3\Pi_{\Omega=0}(v_b, J)$ state molecular constants reported in Refs. 88 and 89, respectively, versus $J(J+1)$. Rotational levels lying near the intersections of the curves are likely to be strongly perturbed. In the present work we used two sets of perturbed levels identified in Refs. 90 and 91: $A(2)^1\Sigma^+(v_A=18, J=26) \sim b(1)^3\Pi_{\Omega=0}(v_b=17, J=26)$ and $A(2)^1\Sigma^+(v_A=20, J=45) \sim b(1)^3\Pi_{\Omega=0}(v_b=18, J=45)$; and two additional sets identified here: $A(2)^1\Sigma^+(v_A=11, J=38) \sim b(1)^3\Pi_{\Omega=0}(v_b=12, J=38)$ and $A(2)^1\Sigma^+(v_A=15, J=15) \sim b(1)^3\Pi_{\Omega=0}(v_b=15, J=15)$. We label each of these intermediate levels by the component [i.e., $A(2)^1\Sigma^+(v_A, J)$ or $b(1)^3\Pi_{\Omega=0}(v_b, J)$] with largest amplitude in the mixed level wave function. Rotational level assignments were confirmed by pumping the same intermediate level from each of the ground state levels $X(1)^1\Sigma^+(v_X=0, J_X=J+1)$ and $X(1)^1\Sigma^+(v_X=0, J_X=J-1)$.

From a particular mixed intermediate window level $A(2)^1\Sigma^+(v_A, J) \sim b(1)^3\Pi_{\Omega=0}(v_b, J)$ we can excite higher lying $1^3\Sigma^+$, $1^3\Pi$, $3^3\Sigma^+$, $3^3\Sigma^-$, $3^3\Pi$, and $3^3\Delta$ states. Singlets can be detected by observation of bound-bound $1^3\Lambda \rightarrow X(1)^1\Sigma^+$ fluorescence in the violet part of the spectrum, while triplets can be detected by the observation of $3^3\Lambda \rightarrow a(1)^3\Sigma^+$ bound-free emission in the green. In addition to the different spectral range in which they radiate, triplets can also be identified since they have greater intensity when excited through the predominantly triplet intermediate level, and most of the triplet levels also exhibit a pronounced hyperfine structure. Levels of the $1^3\Delta$ state, in particular, are identified by their very distinctive fine/hyperfine structure (Fig. 2). We note that $3^3\Delta \rightarrow a(1)^3\Sigma^+$ and $3^3\Sigma^- \rightarrow a(1)^3\Sigma^+$ transitions are dipole forbidden, but double resonance excitation to the $1^3\Delta$ levels can still be detected by collision-induced $3^3\Lambda \rightarrow a(1)^3\Sigma^+$ bound-free emission in the green. However, this collision-induced triplet fluorescence is typically much weaker than direct bound-free triplet fluorescence from upper $3^3\Sigma^+$ and $3^3\Pi$ levels, which are also observed in the present work and that will be reported elsewhere.

$1^3\Delta$ rotational level intensity patterns can be understood by recognizing that the angular momentum coupling scheme of the $1^3\Delta$ state is intermediate between the Hund's case a and case b limits, but much closer to case b than to case a. In the Hund's case b coupling scheme,^{92,93} Λ , the component of electron orbital angular momentum along the internuclear axis, is a good quantum number (see Fig. 2, p. 304, Ref. 93). $\tilde{\Lambda}$ couples to the nuclear rotation vector \tilde{R} to form the vector \tilde{N} . The electron spin \tilde{S} is not coupled strongly to the internuclear axis. Instead, \tilde{S} couples to \tilde{N} to form the total angular momentum (excluding nuclear spin) \tilde{J} . Since $S=1$ for a triplet state, J can take on the values $N-1$, N , and $N+1$ for a given N . The three J levels ($N+1$, N , $N-1$) for given N are labeled F_1 , F_2 , and F_3 , respectively.⁹⁴ Λ doubling for states with $\Lambda \neq 0$ results in a small splitting between J levels with opposite (e/f) parity. Thus we have three sets of e/f level pairs ($J=N-1$, $J=N$, and $J=N+1$) for each distinct value of N .

According to selection rules, $\Delta J=0, \pm 1$ in a dipole transition with $e \leftrightarrow e$, $f \leftrightarrow f$ for $\Delta J = \pm 1$ and $e \leftrightarrow f$ for $\Delta J=0$.⁹⁴

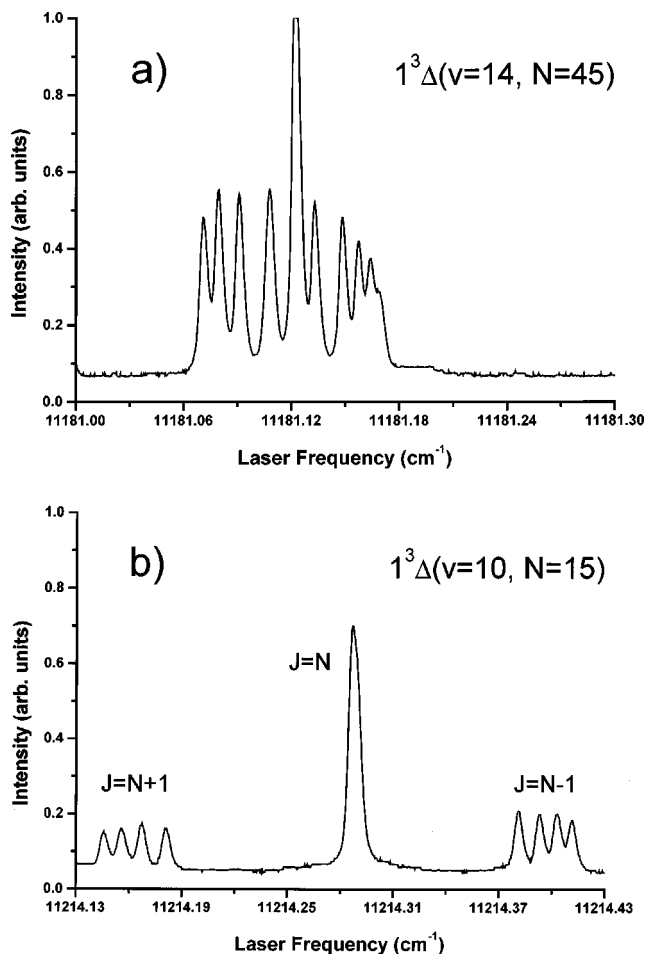


FIG. 2. Fine/hyperfine structure of the $1^3\Delta$ state. (a) $1^3\Delta(v=14, N=45) \leftarrow b(1)^3\Pi_{\Omega=0}(v=18, J=45)$ transition. (b) $1^3\Delta(v=10, N=15) \leftarrow b(1)^3\Pi_{\Omega=0}(v=15, J=15)$ transition. In (b) the $J=N+1$, $J=N$, and $J=N-1$ components are clearly resolved. These spectra were recorded with PUMP and PROBE beams counterpropagating.

Thus, there are nine allowed rotational transitions $1^3\Delta(v_\Delta, N_\Delta, J_\Delta, e/f) \leftarrow b(1)^3\Pi_{\Omega=0}(v_b, J, e)$ from a particular intermediate level $b(1)^3\Pi_{\Omega=0}(v_b, J, e)$ into the $1^3\Delta$ vibrational level v_Δ (see Fig. 3). We note that all $A(2)^1\Sigma^+$ rotational levels have e parity, and due to the $e \leftrightarrow f$ selection rule for perturbations,⁹⁵ we only access e parity $b(1)^3\Pi_{\Omega=0}$ intermediate levels. From Fig. 3 it can be seen that the nine allowed rotational levels are grouped into five sets corresponding to $N_\Delta = J-2, J-1, J, J+1$, and $J+2$. The primary transition labels P , Q , and R correspond to $\Delta J = J_{\text{upper}} - J_{\text{lower}} = -1, 0$, and $+1$, respectively, while subscripts indicate the upper and lower F_1, F_2 , and F_3 components of the transition (i.e., P_{21} represents the $\Delta J = -1$ transition between the upper state F_2 component and lower state F_1 component).

Hyperfine interactions complicate this simple picture, especially at relatively high J , where hyperfine splittings are comparable to the fine splittings between different J levels of the same N manifold. For example, using the intermediate level $b(1)^3\Pi_{\Omega=0}(v_b=18, J=45, e)$ we observe a complicated ten peak fine/hyperfine pattern for the $N_\Delta = J$ transition [see Fig. 2(a)]. Hyperfine structure will be discussed in Sec. III E below. However, at lower J , the fine structure splitting

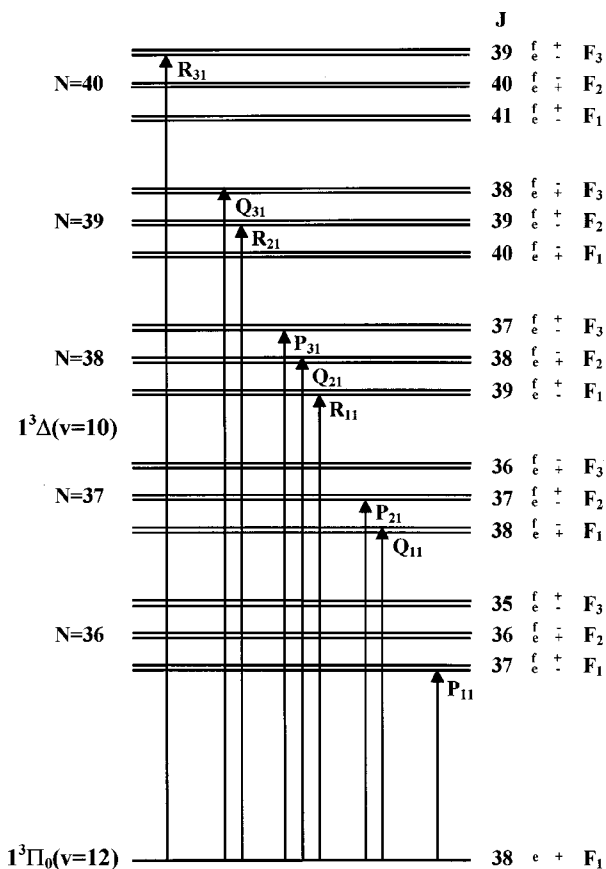


FIG. 3. Allowed rotational transitions from one $^3\Pi_{\Omega=0}(v_{\Pi}, J_{\Pi}, e/f, +/ -)$ lower state level into one vibrational level of a $^3\Delta$ state. In this schematic example, the lower level is taken to be the NaK $b(1)^3\Pi_{\Omega=0}(v=12, J=38, e, +)$ level, which is treated in Hund's case a, while the upper state of the transition is the $v=10$ level of the $1^3\Delta$ state (treated in Hund's case b). (See also Fig. 4.)

is much greater and the rotation line pattern breaks into well-defined J level transitions [Fig. 2(b)], although hyperfine structure is still evident. It can be shown (Ref. 96 and Sec. III E) that the $F_2(J_{\Delta}=N_{\Delta})$ component of the upper state has a much smaller hyperfine splitting than the F_1 and F_3 components. Thus, the F_2 component appears as a single line in Fig. 2(b) while the F_1 and F_3 components display four peak structures with clearly resolved hyperfine splittings. Figure 4 shows the full set of $1^3\Delta(v_{\Delta}=10)$ rotational levels that can be observed from the intermediate level $b(1)^3\Pi_{\Omega=0}(v_b=12, J=38, e)$ [i.e., from the predominantly triplet component of the $A(2)^1\Sigma^+(v_A=11, J=38, e) \sim b(1)^3\Pi_{\Omega=0}(v_b=12, J=38, e)$ mixed pair]. From the selection rules and spectra, it can be seen that the fine structure levels are inverted (i.e., that the highest J within a given N manifold lies lowest). This is consistent with the fact that the dissociation limit of the NaK $1^3\Delta$ state is $\text{Na}(3S) + \text{K}(3D)$, and the atomic $\text{K}(3D)$ fine structure levels are inverted.

B. Molecular constants and RKR potential

A total of 771 $1^3\Delta(v, N, J, e/f)$ levels were identified in the present work with v ranging from 3 to 36. Absolute vibrational numbering was established by a comparison with the recent theoretical potential of Magnier and Millié,⁸⁴ and

by a comparison of calculated and experimental excitation probabilities (see Sec. III C). J values of the levels probed ranged from $J_{\text{intermediate}} - 1$ to $J_{\text{intermediate}} + 1$, while N values ranged from $J_{\text{intermediate}} - 2$ to $J_{\text{intermediate}} + 2$ for the four intermediate levels used in this study ($J_{\text{intermediate}} = 15, 26, 38, 45$). 14 lines were eliminated from further analysis because they were either strongly overlapped by other lines, the signals were extremely noisy, or the assignments were considered to be questionable.

In the first step of the analysis, $1^3\Delta(v, N)$ term values of the 258 $F_2(J=N)$ components were fit to a standard Dunham expansion,^{97,98}

$$E(v, N, J=N) = \sum_{i,k} Y_{i,k} \left(v + \frac{1}{2} \right)^i [N(N+1) - \Lambda^2]^k, \quad (1)$$

with $\Lambda=2$ for the Δ state. To first order, the F_2 components are not affected by the spin-orbit and hyperfine interactions so this analysis yields reasonable values for the molecular constants that are listed in Table I. All realistic diatomic potentials should satisfy the Kratzer relation,^{94,95}

$$Y_{02} = \frac{-4Y_{01}^3}{Y_{10}^2}, \quad (2)$$

while Morse potentials should satisfy the Pekeris relation,^{94,95}

$$Y_{11} = \frac{6Y_{01}^2}{Y_{10}} \left[1 - \left(\frac{-Y_{20}}{Y_{01}} \right)^{1/2} \right]. \quad (3)$$

For the experimental constants listed in Table I, the right hand side of (2) yields $-2.063\text{E}-7$ (compared to $Y_{02} = -2.30\text{E}-7$), while the right hand side of (3) yields $-5.5898\text{E}-4$ (compared to $Y_{11} = -5.0162\text{E}-4$). According to the correlation diagram shown in Fig. 9 of Ref. 32, the dissociation limit of the NaK $1^3\Delta$ state is $\text{Na}(3^2S_{1/2}) + \text{K}(3^2D_{5/2})$. The dissociation energy D_e listed in Table I is based upon this limit.

An attempt was made to fit a first-order Λ doubling constant,⁹⁸ but the fitted value was smaller than its uncertainty. Therefore we did not use Λ doubling constants in the subsequent analysis.

The Dunham coefficients were then used to determine the experimental RKR potential curve,^{102,103} which is shown in Fig. 5. A table (EPAPS Table 1) containing the RKR turning points for the NaK $1^3\Delta$ state has been placed on deposit with the Electronic Physics Auxiliary Publication Service (EPAPS).¹⁰⁴

C. Vibrational numbering and Franck-Condon factors

Due to limitations imposed by the accessible wavelength ranges of the dye and Ti:Sapphire lasers, we were not able to measure level energies all the way down to the bottom of the $1^3\Delta$ potential well. In the analysis described in the preceding section, it was assumed that the lowest $1^3\Delta$ state vibrational level observed in the present work was $v_0=3$. A preliminary assignment of the absolute vibrational numbering was established by comparing the present experimental results with constants derived from the recent theoretical po-

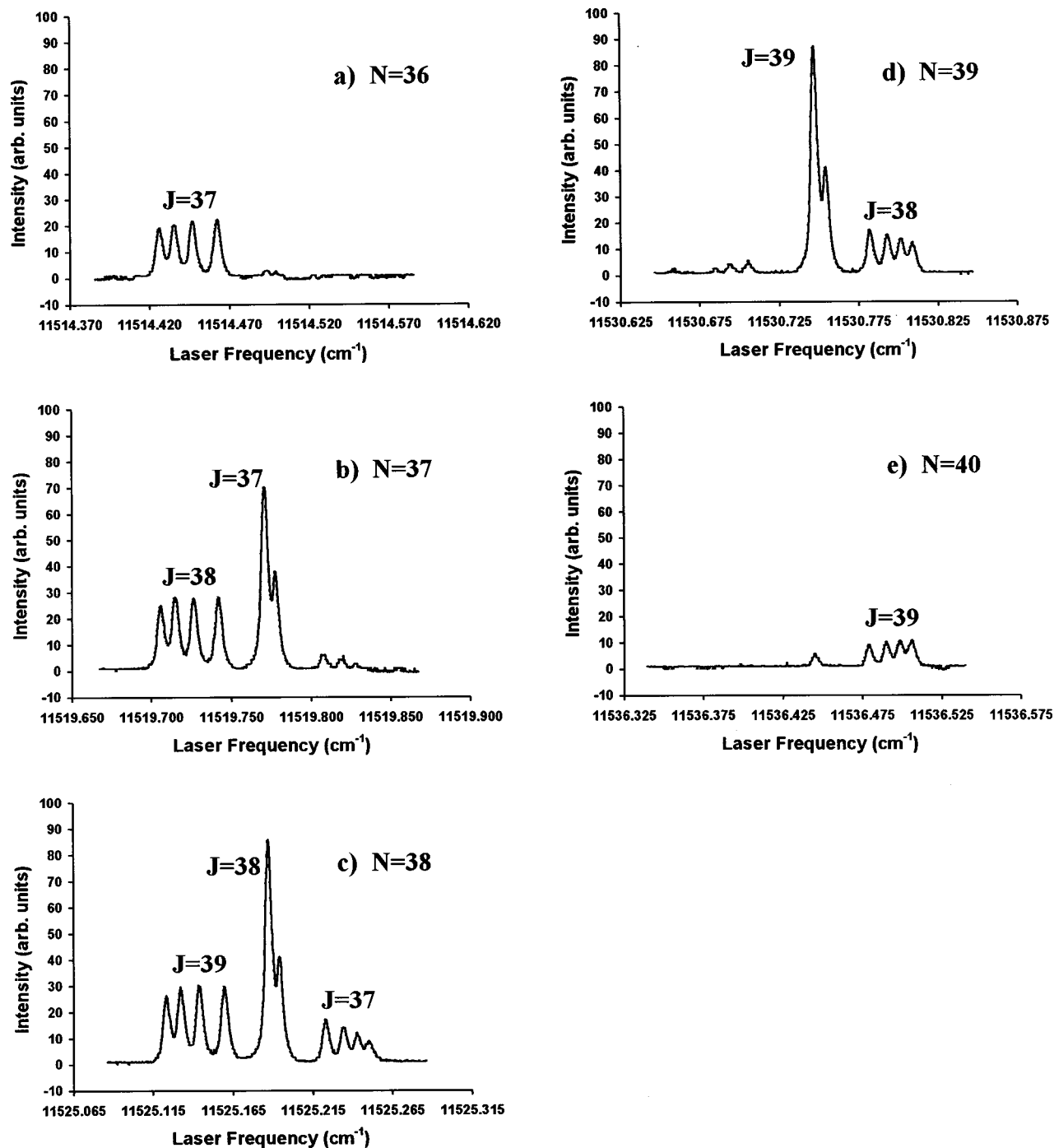


FIG. 4. Rotational transitions into the NaK $1^3\Delta(v=10)$ vibrational level from the $b(1)^3\Pi_{\Omega=0}(v=12, J=38, e, +)$ window level. (a) $N_{\Delta}=36$, $J=37$. (b) $N_{\Delta}=37$, $J=37, 38$. (c) $N_{\Delta}=38$, $J=37, 38, 39$. (d) $N_{\Delta}=39$, $J=38, 39$. (e) $N_{\Delta}=40$, $J=39$. These spectra were recorded with counterpropagating PUMP and PROBE beams.

tentials of Magnier and Millié.⁸⁴ The latter have been shown to give accurate representations of other high-lying states of NaK.^{28,32,35,36,44,82,88,105–109} The assumed numbering, $v_0=3$, gives the best agreement between theoretical and experimental T_e values (Y_{00} in Table I), while $v_0=2$ gives better agreement between vibrational level splittings.

Definite vibrational numbering can be obtained from a comparison of experimental and calculated fluorescence intensities (Franck–Condon factors). Unfortunately, the $1^3\Delta(v_{\Delta}) \rightarrow b(1)^3\Pi$ bound–bound fluorescence is overlapped by very strong $A(2)^1\Sigma^+ \rightarrow X(1)^1\Sigma^+$ fluorescence in-

duced by both the dye and Ti:Sapphire lasers individually. However, we do have a rough measure of $1^3\Delta(v_{\Delta}) \leftarrow b(1)^3\Pi_{\Omega=0}(v_b)$ vibrational line strengths from our double resonance excitation spectra. Experimental excitation line intensities (which are proportional to the absorption line strengths) are generally not as accurate as fluorescence intensities. In the present work, the excitation line intensities depend on relative laser intensities at different wavelengths, exact PUMP laser frequency, beam overlap, etc., compounded by the fact that the excitation spectra were taken on many different days. A single fluorescence spectrum, on the

TABLE I. Molecular constants for the NaK 1³Δ state. Note: All values are given in cm⁻¹ except for the equilibrium internuclear separation R_e which is in Å. The dissociation energy D_e was obtained from the expression $D_e = [D_e(X^1\Sigma^+) + \Delta E_{\text{atomic}} - Y_{00}]$ with $D_e(X^1\Sigma^+) = (5274.9 \pm 0.5) \text{ cm}^{-1}$ from Ref. 100 and $\Delta E_{\text{atomic}} = E[\text{Na}(3S_{1/2}) + \text{K}(3D_{5/2})] - E[\text{Na}(3S_{1/2}) + \text{K}(4S_{1/2})] = 21\,534.42$ from Ref. 101. Quoted uncertainties represent 95% confidence limits.

	Experiment (this work)	Theory
R_e	3.8816 ± 0.0012	3.89 ^{a,b}
D_e	3201.5 ± 0.5	3075 ^{a,b}
Y_{00}	23 607.8621 ± 0.0380	23 647 ^a 23 653 ^b
Y_{10}	94.790 87 ± 0.007 90	93.60 ^a 93.23 ^b
Y_{20}	-0.473 925 ± 0.000 530	
Y_{30}	-1.271E-03 ± 1.6E-05	
Y_{40}	-5.107E-05 ± 1.9E-07	
Y_{01}	0.077 382 6 ± 0.000 048 0	
Y_{11}	-5.0162E-04 ± 5.60E-06	
Y_{21}	4.5E-07 ± 2.1E-07	
Y_{31}	-1.920E-07 ± 3.4E-09	
Y_{02}	-2.30E-07 ± 2.5E-08	
Y_{12}	1.9E-09 ± 2.6E-09	
Y_{22}	-1.80E-10 ± 6.1E-11	
A_0	-0.234 91 ± 0.001 32	
A_1	-0.001 24 ± 0.000 07	

^aReference 84.

^bReference 99.

other hand, can be taken in a few minutes with no adjustments made to either laser, and only the relative detection system efficiency versus wavelength needs to be calibrated. Nevertheless, the absorption spectra still give a reasonable picture of weak and strong vibrational transitions and can certainly identify upper state vibrational levels for which the relevant Franck–Condon factor is negligible.

The intensity of an absorption line, $I_{\text{abs.}}$, is given by⁹²

$$I_{\text{abs.}}(v' \leftarrow v'') \propto \nu \left| \int \psi_{v'} M_e(R) \psi_{v''} dR \right|^2. \quad (4)$$

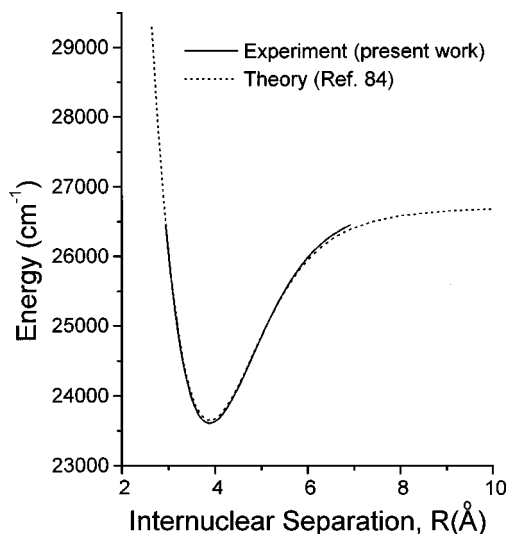


FIG. 5. Comparison between experimental and theoretical NaK 1³Δ state potential curves. Dotted line: theoretical potential from Ref. 84. Solid line: experimental potential obtained in the present work.

Here ν is the line frequency, $\psi_{v'}$ and $\psi_{v''}$ are the upper and lower level radial wave functions, respectively, and $M_e(R)$ is the transition dipole moment as a function of internuclear separation R .

We carried out calculations of absorption line intensities using each of the assumed vibrational numbering schemes $v_0=2$, $v_0=3$, and $v_0=4$. In each case, a set of Dunham coefficients was calculated using the DSParFit program.⁹⁸ These constants were then used to generate a candidate RKR potential using the program RKR1.¹⁰³ Finally, absorption line intensities were calculated using the program LEVEL 6.0.¹¹⁰ In these last calculations, the NaK 1³Δ ← $b(1)^3\Pi$ transition dipole moment was taken from Ref. 99. The results of these calculations are shown in Fig. 6 for 1³Δ($v_\Delta, J=N=26$) ← $b(1)^3\Pi_{\Omega=0}(v_b=17, J=26)$ transitions, where they are compared to the relative experimental excitation line intensities. Although the level of agreement between experimental and calculated intensities is marginal in all cases for the reasons given above, it is clear that the node positions are much more accurately reproduced using the assignment $v_0=3$. Similar results were obtained for 1³Δ($v_\Delta, J=N=15$) ← $b(1)^3\Pi_{\Omega=0}(v_b=15, J=15)$, 1³Δ($v_\Delta, J=N=38$) ← $b(1)^3\Pi_{\Omega=0}(v_b=12, J=38)$, and 1³Δ($v_\Delta, J=N=45$) ← $b(1)^3\Pi_{\Omega=0}(v_b=18, J=45)$ transitions. Thus we believe that the assignment $v_0=3$ most likely provides the correct vibrational numbering for the NaK 1³Δ state.

D. Spin–orbit constant

As stated earlier, the angular momentum coupling scheme of the NaK 1³Δ state is intermediate between Hund’s case a and Hund’s case b, but much closer to case b. Nevertheless, it is most convenient to start from the case a wave functions when analyzing the 1³Δ state fine structure. Either case b or case a basis functions can be used in the analysis, as long as the full spin-dependent Hamiltonian is diagonalized for a given v_Δ and J . Figure 1, p. 298, Ref. 93 shows the Hund’s case a angular momentum coupling scheme. In case a, the electron spin \vec{S} is considered to be strongly coupled to the internuclear axis with component Σ . Σ and Λ add together to form Ω (the total electronic angular momentum along the internuclear axis). $\vec{\Omega}$ then couples to the nuclear rotation vector \vec{R} to form the vector \vec{J} . Case a basis functions for a given J are labeled by the value of Ω . For the 1³Δ state, $\Lambda = 2$ and $\Sigma = -1, 0, +1$. Thus $\Omega = 1, 2$, and 3.

According to Refs. 111 and 112, the case a Hamiltonian matrix for a ³Δ state with given vibrational state v and rotational quantum number J , has the following components $H_{\Omega\Omega'}$:

$$H_{11} = T_\Delta - 2A_\Delta + B_\Delta x - D_\Delta(x^2 + 2x - 4) + \epsilon - \gamma,$$

$$H_{22} = T_\Delta + B_\Delta(x - 2) - D_\Delta(x^2 - 12) - 2\epsilon - 2\gamma,$$

$$H_{33} = T_\Delta + 2A_\Delta + B_\Delta(x - 8) - D_\Delta(x^2 - 14x + 52)$$

$$+ \epsilon - \gamma,$$

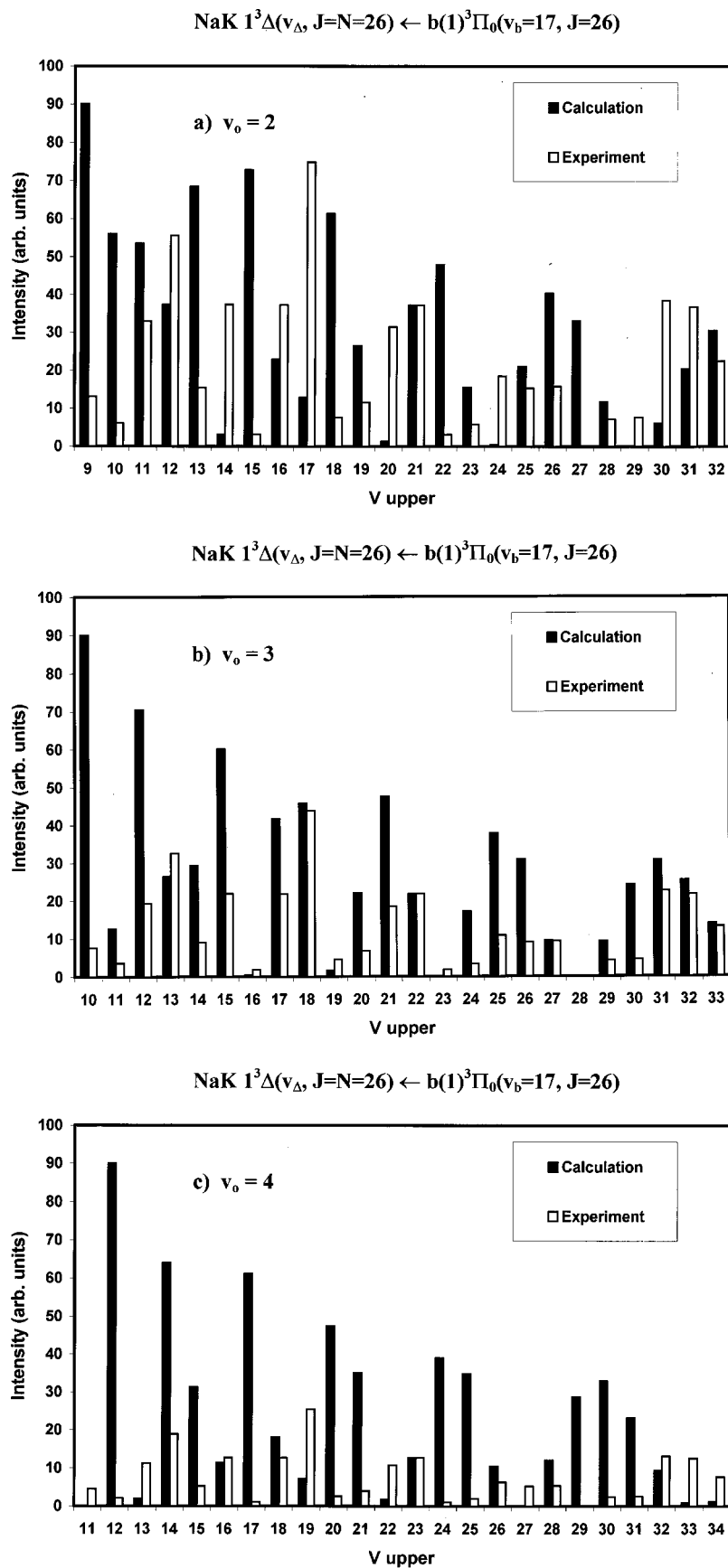


FIG. 6. Comparison between experimental and calculated $1^3\Delta(v_\Delta, J=N=26) \leftarrow b(1)^3\Pi_{\Omega=0}(v_b=17, J=26)$ absorption line intensities for various assignments of the lowest observed $1^3\Delta$ state vibrational level v_0 . (a) $v_0=2$; (b) $v_0=3$; (c) $v_0=4$. In each case, the calculated intensity is given by $v|\int \psi_v' M_e(R) \psi_v'' dR|^2$ using the calculated $1^3\Delta \leftarrow b(1)^3\Pi$ transition dipole moment from Ref. 99. The experimental and calculated intensities are normalized to each other at $v=21$, $v=22$, and $v=23$, in parts (a), (b), and (c), respectively.

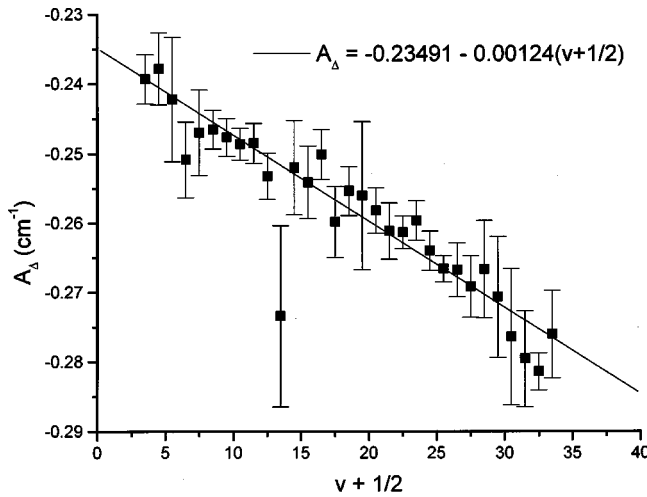


FIG. 7. Measured A_{Δ} values (with error bars), obtained from least-squares fitting of experimental term values using the LSQ program, plotted against $(v + 1/2)$. Solid line is a linear fit to the function $A_{\Delta} = A_0 + A_1(v + \frac{1}{2})$ with $A_0 = -0.23491$ and $A_1 = -0.00124$.

$$\begin{aligned}
 H_{12} &= B_{\Delta}(2x-4)^{1/2} - 2D_{\Delta}(x-1)(2x-4)^{1/2} \\
 &\quad - \frac{\gamma}{\sqrt{2}}(x-2)^{1/2}, \\
 H_{23} &= B_{\Delta}(2x-12)^{1/2} - 2D_{\Delta}(x-5)(2x-12)^{1/2} \\
 &\quad - \frac{\gamma}{\sqrt{2}}(x-6)^{1/2}, \\
 H_{13} &= -2D_{\Delta}(x^2 - 8x + 12)^{1/2}.
 \end{aligned} \tag{5}$$

In these expressions, $x \equiv J(J+1)$, T_{Δ} is the electronic/vibrational energy, B_{Δ} is the rotational constant, D_{Δ} is the centrifugal distortion constant, A_{Δ} is the spin-orbit constant, γ is the spin-rotation constant, and ϵ is the spin-spin constant,^{111,112} respectively, for the NaK $1^3\Delta$ state.

We used the computer program LSQ⁸⁵ to analyze the full set of measured rotational level energies (F_1 , F_2 , and F_3 components) for each $1^3\Delta$ vibrational level. For each component, we use the weighted mean of the observed hyperfine lines. The LSQ program carries out the matrix diagonalization and varies the fitting parameters to give the best least-squares fit to the input data. In our use of the program, the constants T_{Δ} , B_{Δ} , and D_{Δ} were fixed at the values determined from the earlier Dunham fit of the F_2 components. A_{Δ} , γ , and ϵ were allowed to vary in the fit. However, values for the spin-rotation and spin-spin constants were always found to be less than their uncertainties and these constants were set to zero in the subsequent analysis. Thus, in the final fits, only the parameter A_{Δ} was allowed to vary although the fitted values of A_{Δ} were not significantly changed if γ and ϵ were included in the fit, or if the constants T_{Δ} , B_{Δ} , and D_{Δ} were also allowed to vary. Fitted values of A_{Δ} are plotted in Fig. 7, where it can be seen that they display a weak linear dependence on v . This fitting procedure thus yields the NaK $1^3\Delta$ state spin-orbit interaction constants, given by

$$\begin{aligned}
 A_{\Delta} &= A_0 + A_1(v + 1/2) \\
 &= [-0.23491 - 0.00124(v + 1/2)] \text{ cm}^{-1}.
 \end{aligned} \tag{6}$$

Calculated term values based on the molecular constants listed in Table I, including the spin-orbit constants, reproduce the 757 NaK $1^3\Delta$ state term values measured in this work with a root mean square discrepancy of 0.009 cm^{-1} . All measured NaK $1^3\Delta(v, N, J)$ level energies, with comparisons to energies calculated using the constants reported in Table I, are listed in EPAPS Table 2 of the supplementary Electronic Physics Auxiliary Publication Service (EPAPS) document.¹⁰⁴ Also listed in EPAPS Table 2 are the ground state, intermediate state and upper ($1^3\Delta$) state levels, and PUMP and PROBE laser frequencies for each PFOODR transition studied in this work.

E. Hyperfine structure

Hyperfine structure is readily observable in this experiment because the double resonance technique using narrow-band lasers is inherently Doppler free. The NaK ground state $X(1)^1\Sigma^+$ is expected to have negligible hyperfine structure^{83,113} since $S=0$ and $\Lambda=0$ (see the discussion below). Therefore, the pump laser resonance condition is

$$\begin{aligned}
 \hbar \omega_{\text{PUMP}} &= E[b(1)^3\Pi_{\Omega=0}(v_b, J_b, F_b)] \\
 &\quad - E[X(1)^1\Sigma^+(v_X, J_X)] + \hbar \vec{k}_{\text{PUMP}} \cdot \vec{v} \\
 &= E[b(1)^3\Pi_{\Omega=0}(v_b, J_b, F_b)] \\
 &\quad - E[X(1)^1\Sigma^+(v_X, J_X)] + \frac{\hbar \omega_{\text{PUMP}} n_{\text{PUMP}} v_z}{c},
 \end{aligned} \tag{7}$$

where ω_{PUMP} and \vec{k}_{PUMP} are the PUMP laser frequency and wave vector, n_{PUMP} is the index of refraction of the vapor at ω_{PUMP} , and \vec{v} is the molecular velocity. $E[b(1)^3\Pi_{\Omega=0}(v_b, J_b, F_b)]$ is the energy of the $b(1)^3\Pi_{\Omega=0}(v_b, J_b, F_b)$ hyperfine level, and $E[X(1)^1\Sigma^+(v_X, J_X)]$ is the energy of the initial $X(1)^1\Sigma^+(v_X, J_X)$ level. Here, the PUMP laser propagation direction is chosen to be the z axis. Thus only one velocity group (i.e., those molecules with a z component of velocity v_z) will be excited for each intermediate state hyperfine level F_b .

The PROBE laser resonance condition is similarly given by the expression

$$\begin{aligned}
 \hbar \omega_{\text{PROBE}} &= E[(1)^3\Delta(v_{\Delta}, N_{\Delta}, J_{\Delta}, F_{\Delta})] \\
 &\quad - E[b(1)^3\Pi_{\Omega=0}(v_b, J_b, F_b)] + \hbar \vec{k}_{\text{PROBE}} \cdot \vec{v} \\
 &= E[(1)^3\Delta(v_{\Delta}, N_{\Delta}, J_{\Delta}, F_{\Delta})] \\
 &\quad - E[b(1)^3\Pi_{\Omega=0}(v_b, J_b, F_b)] \\
 &\quad + \frac{\hbar \omega_{\text{PROBE}} n_{\text{PROBE}} v_z}{c},
 \end{aligned} \tag{8}$$

where ω_{PROBE} and \vec{k}_{PROBE} are the PROBE laser frequency and wave vector, n_{PROBE} is the index of refraction of the vapor at ω_{PROBE} , and $E[(1)^3\Delta(v_{\Delta}, N_{\Delta}, J_{\Delta}, F_{\Delta})]$ is the en-

ergy of the level $1^3\Delta(v_\Delta, N_\Delta, J_\Delta, F_\Delta)$. The upper (minus) sign in Eq. (8) corresponds to the case of counterpropagating lasers (PROBE propagating in the $-z$ direction) and the lower (plus) sign to the case of copropagating lasers.

We define $E[b(1)^3\Pi_{\Omega=0}(v_b, J_b)]$ and $E[(1)^3\Delta(v_\Delta, N_\Delta, J_\Delta)]$ to be the weighted means of the $b(1)^3\Pi_{\Omega=0}(v_b, J_b, F_b)$ and $1^3\Delta(v_\Delta, N_\Delta, J_\Delta, F_\Delta)$ hyperfine components, respectively. If we assume for simplicity that the PUMP laser is fixed to line center of the $b(1)^3\Pi_{\Omega=0}(v_b, J_b) \leftarrow X(1)^1\Sigma^+(v_X, J_X)$ transition, $\hbar\omega_{\text{PUMP}} = E[b(1)^3\Pi_{\Omega=0}(v_b, J_b)] - E[X(1)^1\Sigma^+(v_X, J_X)]$, and that the indices of refraction n_{PUMP} and n_{PROBE} are both equal to 1, we can eliminate v_z from Eqs. (7) and (8) and obtain the PROBE laser resonance condition:

$$\begin{aligned} \hbar\omega_{\text{PROBE}} - \{ & E[(1)^3\Delta(v_\Delta, N_\Delta, J_\Delta)] \\ & - E[b(1)^3\Pi_{\Omega=0}(v_b, J_b)] \} \\ = \{ & E[(1)^3\Delta(v_\Delta, N_\Delta, J_\Delta, F_\Delta)] \\ & - E[(1)^3\Delta(v_\Delta, N_\Delta, J_\Delta)] \} - \left\{ 1 \mp \frac{\omega_{\text{PROBE}}}{\omega_{\text{PUMP}}} \right\} \\ \times \{ & E[b(1)^3\Pi_{\Omega=0}(v_b, J_b, F_b)] \\ & - E[b(1)^3\Pi_{\Omega=0}(v_b, J_b)] \}. \end{aligned} \quad (9)$$

For the case of counterpropagating lasers [the minus sign in Eq. (9)], and in the limit that $\omega_{\text{PROBE}} \approx \omega_{\text{PUMP}}$ we see that the intermediate $b(1)^3\Pi_{\Omega=0}$ state hyperfine structure drops out, and the probe laser simply traces out the hyperfine structure of the upper state as it is scanned around the weighted mean of the $1^3\Delta(v_\Delta, N_\Delta, J_\Delta) \leftarrow b(1)^3\Pi_{\Omega=0}(v_b, J_b)$ transition. In the present case, $0.81 < \omega_{\text{PROBE}}/\omega_{\text{PUMP}} < 0.96$. Thus, the counterpropagating geometry facilitates the observation of the upper $1^3\Delta$ state hyperfine structure, by canceling most of the contribution from the $b(1)^3\Pi_{\Omega=0}$ state.

In the copropagating case [the plus sign in Eq. (9)], we see that both the $1^3\Delta$ state and the $b(1)^3\Pi_{\Omega=0}$ state hyperfine structures contribute to the observed line spacings. In the limit that $\omega_{\text{PROBE}} \approx \omega_{\text{PUMP}}$ the line spacings will reflect the $1^3\Delta$ state hyperfine structure minus twice the $b(1)^3\Pi_{\Omega=0}$ state hyperfine structure. Thus, the difference between the line spacings in the co- and counterpropagating geometries allows the $b(1)^3\Pi_{\Omega=0}$ state hyperfine structure to be studied. Examples of spectra recorded with the co- and counterpropagating PUMP/PROBE geometries are shown in Fig. 8.

According to Ref. 114, the diagonal matrix elements of the Fermi contact interaction (see below) are expected to be negligible for the $b(1)^3\Pi_{\Omega=0}$ state. However, the $\Omega=1$ and $\Omega=2$ components have nonzero diagonal matrix elements, and the $b(1)^3\Pi_{\Omega=0}$ state might acquire appreciable hyperfine structure from mixing of the three fine structure components as the rotation number increases.⁸² In Ref. 115, for example, the analogous $\text{Na}_2^3\Pi_{\Omega=0,u}$ state was found to have hyperfine structure splittings that are comparable to those of the $^3\Pi_{\Omega=2,u}$ state and much larger than those for the $^3\Pi_{\Omega=1,u}$ state. In addition, perturbations between $b(1)^3\Pi_{\Omega=0}$ and other states can result in appreciable hyperfine structure. Ishikawa *et al.*⁸³ report NaK $b(1)^3\Pi_{\Omega=0}(v \sim 62)$ state total hyperfine splittings (i.e., splittings between

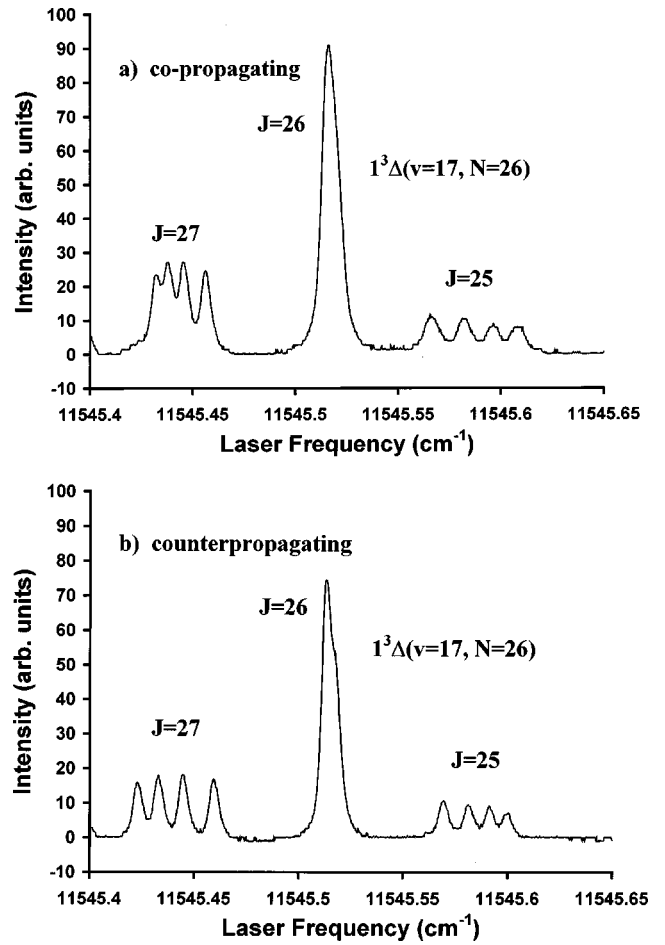


FIG. 8. Fine and hyperfine structure of the $1^3\Delta(v_\Delta=17, N_\Delta=26) \leftarrow b(1)^3\Pi_{\Omega=0}(v_b=17, J_b=26)$ transition recorded with the PROBE laser (a) copropagating and (b) counterpropagating with the PUMP laser. In part (b) the observed hyperfine structure is primarily that of the upper $1^3\Delta$ state. In part (a) the observed hyperfine structure is that of the upper $1^3\Delta$ state minus approximately twice that of the intermediate $b(1)^3\Pi_{\Omega=0}$ level. Since the hyperfine structure of the $1^3\Delta(v_\Delta=17, N_\Delta=26, J_\Delta=25)$ level is inverted, the intermediate level hyperfine structure (multiplied by $\{1 + \omega_{\text{PROBE}}/\omega_{\text{PUMP}}\}$) increases the observed splittings relative to those in the counterpropagating case. For the $1^3\Delta(v_\Delta=17, N_\Delta=26, J_\Delta=27)$ level, which is not inverted, the observed splittings are compressed.

the lowest- and highest-frequency hyperfine components of a line) of up to $\sim 0.02 \text{ cm}^{-1}$, but only in the range $15 < J < 30$, where the $b(1)^3\Pi_{\Omega=0}(v \sim 62)$ state is strongly perturbed by the $c(2)^3\Sigma^+$ state. From a comparison of Figs. 8(a) and 8(b), we can estimate that the total splitting of the NaK $b(1)^3\Pi_{\Omega=0}(v=17, J=26, e, +)$ level is approximately 0.0060 cm^{-1} . A detailed analysis of the NaK $b(1)^3\Pi$ state hyperfine structure would require more data obtained with the copropagating geometry.

The magnetic hyperfine structure Hamiltonian for a diatomic molecule described in Hund's case a or b can be written as^{82,96,116}

$$\begin{aligned} H_{\text{hfs}} = \sum_{i,n} & [a\Lambda\vec{I}(n) \cdot \vec{k} + (b-c)\vec{I}(n) \cdot \vec{S}(i) \\ & + 3c(\vec{I}(n) \cdot \vec{k})(\vec{S}(i) \cdot \vec{k})], \end{aligned} \quad (10)$$

where

$$\begin{aligned}
 a &= 2\mu_{\text{B}}g_I\mu_N \left\langle \frac{1}{r_{in}^3} \right\rangle_{\text{ave}}, \\
 b &= \frac{16\pi}{3} \mu_{\text{B}}g_I\mu_N |\psi(r_{in}=0)|^2, \\
 c &= \mu_{\text{B}}g_I\mu_N \left\langle \frac{3 \cos^2 \theta - 1}{r_{in}^3} \right\rangle_{\text{ave}}.
 \end{aligned}
 \tag{11}$$

Here μ_{B} , g_I , and μ_N represent the Bohr magneton, the g value for nucleus n , and the nuclear magneton, respectively. \vec{k} is a unit vector along the internuclear axis, \vec{r}_{in} is the vector separation between nucleus n and electron i , $|\psi(r_{in}=0)|^2$ is the probability of finding electron i at the position of nucleus n , and θ is the angle between the internuclear axis and the vector \vec{r}_{in} . $\vec{S}(i)$ and $\vec{I}(n)$ are the spin angular momenta of electron i and nucleus n , respectively. The term $b\vec{I}\cdot\vec{S}$ represents the Fermi contact interaction, while the a and c terms represent the nuclear spin–electron orbital angular momentum interaction, and the nuclear spin–electron spin dipole interaction, respectively.

The sum in expression (10) runs over all electrons in the molecule and both nuclei. However, electrons occupying filled shells do not contribute since $\Lambda=0$ and $S=0$ for those electrons. The probability $|\psi(r_{in}=0)|^2$ of finding the electron at the position of the nucleus is negligible unless there is an appreciable amount of atomic s state orbital in the wave function of an unpaired electron. Conversely, when there is an appreciable amount of atomic s state orbital in the electron wave function, the Fermi contact term usually dominates the magnetic hyperfine interaction.^{74,83,96,117} In the present case, the NaK 1³Δ state dissociates to the Na(3s²S_{1/2}) + K(3d²D_{5/2}) asymptotic limit. Thus, the hyperfine structure of this state should be dominated by the Fermi contact interaction involving the sodium atom nucleus ($I=\frac{3}{2}$).⁷⁴ Under these circumstances, interactions involving the electric quadrupole moments of the nuclei can also be neglected.

Evaluation of the hyperfine energies from the Hamiltonian given in Eq. (10) depends on the angular momentum coupling scheme followed in the case of interest. The NaK 1³Δ state is close to Hund’s case b, where the electron spin is not coupled strongly to the internuclear axis. If the nuclear spin angular momentum is also not coupled strongly to the internuclear axis then the coupling case is called b_{β} and two subcases are possible. In case $b_{\beta S}$, \vec{S} , and \vec{I} couple to form an intermediate vector \vec{G} ($\vec{S}+\vec{I}=\vec{G}$) and then \vec{G} couples to \vec{N} to form the total angular momentum vector \vec{F} ($\vec{G}+\vec{N}=\vec{F}$). In case $b_{\beta J}$, \vec{S} first couples to \vec{N} to form \vec{J} ($\vec{S}+\vec{N}=\vec{J}$) and \vec{I} then couples to \vec{J} to form the total angular momentum vector \vec{F} ($\vec{I}+\vec{J}=\vec{F}$). The case $b_{\beta S}$ and $b_{\beta J}$ coupling schemes are illustrated in Fig. 5 of Ref. 47 (or Fig. 8-1 in Ref. 96). For the NaK 1³Δ state and low rotation quantum number N , J is approximately a good quantum number [see Fig. 2(b)] and the $b_{\beta J}$ coupling scheme is valid. At higher N values [Fig. 2(a)], the coupling scheme is intermediate between cases $b_{\beta S}$ and $b_{\beta J}$.

In the case $b_{\beta J}$ limit, and for $S=1$, the Fermi contact interaction hyperfine splittings are given by⁹⁶

$$E_{J=N+1} = \frac{b}{2(N+1)} [F(F+1) - I(I+1) - J(J+1)]\hbar^2,
 \tag{12}$$

$$E_{J=N} = \frac{b}{2N(N+1)} [F(F+1) - I(I+1) - J(J+1)]\hbar^2,
 \tag{13}$$

$$E_{J=N-1} = \frac{-b}{2N} [F(F+1) - I(I+1) - J(J+1)]\hbar^2.
 \tag{14}$$

These results can be understood from a simple vector coupling model.¹¹⁴ In case $b_{\beta J}$ \vec{S} and \vec{N} precess rapidly around \vec{J} and only S_J , the component of the electron spin along \vec{J} , contributes to the effective spin dipole moment. Thus, the coupling term becomes $b\vec{I}\cdot\vec{S} = b\vec{I}\cdot\vec{S}_J = b\vec{I}\cdot\vec{J}(S_J/|\vec{J}|)$. For $J=N+1$ we have $|\vec{J}|=[J(J+1)]^{1/2}\hbar$ and $|\vec{N}|=[N(N+1)]^{1/2}\hbar = [(J-1)J]^{1/2}\hbar$, while $|\vec{S}|=[S(S+1)]^{1/2}\hbar = [2]^{1/2}\hbar$ for $S=1$. From the geometry of Fig. 18 (F_1 component) of Ref. 114, we can therefore see that

$$\begin{aligned}
 |\vec{S}|^2 - S_J^2 &= S_{\perp}^2 \\
 &= |\vec{N}|^2 - [|\vec{J}| - S_J]^2 \\
 &= [(J-1)J]\hbar^2 - [[J(J+1)]^{1/2}\hbar - S_J]^2, \\
 2\hbar^2 - S_J^2 &= -2J\hbar^2 + 2S_J[J(J+1)]^{1/2}\hbar - S_J^2,
 \end{aligned}
 \tag{15}$$

where S_J and S_{\perp} represent the components of the vector \vec{S} along \vec{J} and perpendicular to \vec{J} , respectively. Equation (15) then yields

$$\frac{S_J}{|\vec{J}|} = \frac{(J+1)\hbar}{|\vec{J}|[J(J+1)]^{1/2}} = \frac{1}{J} = \frac{1}{N+1}.
 \tag{16}$$

Since $\vec{I}\cdot\vec{J} = \frac{1}{2}[F(F+1) - I(I+1) - J(J+1)]\hbar^2$, this result leads directly to Eq. (12). In a similar fashion, the F_2 and F_3 diagrams of Fig. 18, Ref. 114 lead directly to Eqs. (13) and (14). Note that the extra factor of N in the denominator of Eq. (13) [as compared to Eq. (12)] causes the hyperfine splittings of F_2 components ($J=N$ components) to be more than an order of magnitude smaller than those of F_1 and F_3 components, for all N values used in the present study. This is readily observable in Fig. 2(b), where the F_2 component hyperfine structure is not resolved while the hyperfine structure of the F_1 and F_3 components is clearly resolved.

As stated above, the dominant contribution to the NaK 1³Δ state hyperfine structure is the Fermi contact interaction between the unpaired electron spins and the sodium nuclear spin. Since the sodium nuclear spin quantum number is $I=\frac{3}{2}$, we expect each rotational level J to split into four components: $F=J-\frac{3}{2}$, $J-\frac{1}{2}$, $J+\frac{1}{2}$, and $J+\frac{3}{2}$.

In the case $b_{\beta J}$ coupling scheme, we see from Eqs. (12)–(14) that each of the three fine structure components (F_1 , F_2 , and F_3) of an N manifold obey a Landé interval rule:

$$\Delta E_{\text{hfs}}(J, F) = E(J, F) - E(J, F-1) = \alpha_J F,
 \tag{17}$$

with

$$\begin{aligned}\alpha_{J=N+1} &= \frac{b\hbar^2}{N+1}, \\ \alpha_{J=N} &= \frac{b\hbar^2}{N(N+1)}, \\ \alpha_{J=N-1} &= \frac{-b\hbar^2}{N}.\end{aligned}\quad (18)$$

Thus, we expect that the F_1 component ($J=N+1$) will display four lines with spacings of $\alpha_{J=N+1}(J-\frac{1}{2})$, $\alpha_{J=N+1}(J+\frac{1}{2})$, and $\alpha_{J=N+1}(J+\frac{3}{2})$, in order of increasing energy, or $b\hbar^2(N+\frac{1}{2})/(N+1)$, $b\hbar^2(N+\frac{3}{2})/(N+1)$, and $b\hbar^2(N+\frac{5}{2})/(N+1)$. Similarly, the F_3 component ($J=N-1$) will be inverted, with spacings of $-\alpha_{J=N-1}(J+\frac{3}{2})$, $-\alpha_{J=N-1}(J+\frac{1}{2})$, and $-\alpha_{J=N-1}(J-\frac{1}{2})$, or $b\hbar^2(N+\frac{1}{2})/N$, $b\hbar^2(N-\frac{1}{2})/N$, and $b\hbar^2(N-\frac{3}{2})/N$. Finally, the F_2 component will also display four lines with spacings of $\alpha_{J=N}(J-\frac{1}{2})$, $\alpha_{J=N}(J+\frac{1}{2})$, and $\alpha_{J=N}(J+\frac{3}{2})$, or $b\hbar^2(N-\frac{1}{2})/[N(N+1)]$, $b\hbar^2(N+1/2)/[N(N+1)]$, and $b\hbar^2(N+3/2)/[N(N+1)]$.

Transitions to the NaK $1^3\Delta$ state rotational levels $N=13-17$ from the intermediate state window level $A(2)^1\Sigma^+(v_A=15, J=15) \sim b(1)^3\Pi_{\Omega=0}(v_b=15, J=15)$, recorded with the counterpropagating PUMP/PROBE geometry, were used to analyze the $1^3\Delta$ state hyperfine structure, since these represent the lowest rotational levels studied, and thus most closely approximate the case $b_{\beta J}$ coupling scheme. In all cases, the hyperfine structure of the F_2 components was unresolved [see Fig. 2(b)]. However, an analysis of 378 line splittings in the F_1 and F_3 components allowed us to determine the value

$$b\hbar^2 \approx 0.0111 \text{ cm}^{-1}. \quad (19)$$

Deviations from the Landé interval rule are on the order of 10%. Such deviations result from residual hyperfine structure of the $b(1)^3\Pi_{\Omega=0}$ intermediate state level that does not cancel out completely, even in the counterpropagating geometry, due to the unequal frequencies of the PUMP and PROBE lasers, and from neglect of various small contributions to the $1^3\Delta$ state hyperfine structure. The latter include the Fermi contact term associated with the potassium atom nucleus (which contributes if the molecular $1^3\Delta$ state wave function has a nonzero contribution from a potassium atom s orbital), nuclear spin–electron orbital and nuclear spin–electron spin magnetic dipole interactions, and interactions involving the electric quadrupole moments of the nuclei. In addition, we can see from Fig. 2(a) that at high N the hyperfine splittings become comparable to the fine structure splittings. Thus, J is not a good quantum number in this limit and the hyperfine structure must be considered to be intermediate between the $b_{\beta J}$ and $b_{\beta S}$ coupling limits. One could, in principle, extend the Hund's case a matrix elements of Eq. (5) to include hyperfine interactions (using, for example, case a_α basis functions), and diagonalize the resulting 12×12 matrix. Such an analysis might need to include spin–spin and spin–rotation interactions as well as the so-far-neglected hyperfine interactions. We have not attempted this analysis in the present case because it appears unlikely that it would result in a significantly improved value for the $1^3\Delta$ state Fermi contact interaction constant reported above.

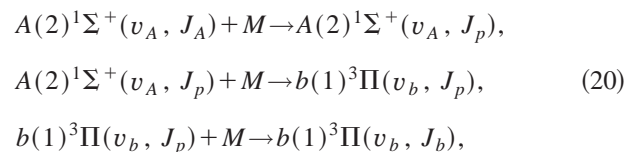
The value of the constant representing the Fermi contact interaction between the electron spin and the sodium nucleus for the NaK $1^3\Delta$ state reported in Eq. (19) above is consistent with the values 0.0104, 0.0112, 0.0108, and 0.0105 cm^{-1} reported in Refs. 73, 81, 82, and 83, respectively, for the NaK $c(2)^1\Sigma^+$ state. Reference 74 gives the value 0.0142 cm^{-1} for the Fermi contact interaction between the electron spin and sodium nucleus in the NaK $a(1)^3\Sigma^+$ state.

As mentioned above, for higher N values, J is no longer strictly a good quantum number. This can be seen in Figs. 4(a), 4(b), 4(d), and 4(e), where very weak $\Delta J = \pm 2$ transitions are clearly visible from the intermediate level $b(1)^3\Pi_{\Omega=0}(v=12, J=38, e, +)$. However, F is always a good quantum number and in Figs. 4(b) and 4(d) we see that only three such “forbidden” $\Delta J = \pm 2$ lines are observed in each case. In Fig. 4(d), for example, the $1^3\Delta(J=40)$ level is split into four hyperfine levels with $F=41.5, 40.5, 39.5$, and 38.5 . According to the $\Delta F=0, \pm 1$ selection rule, only the last three of these can be accessed from $b(1)^3\Pi_{\Omega=0}(J=38)$, for which $F=39.5, 38.5, 37.5$, and 36.5 .

F. Gateway effect

In this work we observed strong collisional transfer of population from one member of a mutually perturbing $A(2)^1\Sigma^+(v_A, J) \sim b(1)^3\Pi(v_b, J)$ pair of levels to the other member. Specifically, we found that we could PUMP the predominantly singlet member of the mutually perturbing pair from the ground state, $A(2)^1\Sigma^+(v_A, J) \leftarrow X(1)^1\Sigma^+(v_X, J \pm 1)$, and then PROBE on the $1^3\Delta(v_\Delta, N_\Delta, J_\Delta) \leftarrow b(1)^3\Pi(v_b, J)$ transition starting from the predominantly triplet member of the pair, or *vice versa*. These collision-assisted transitions to the $1^3\Delta$ state were important to our data analysis because they provided the only recorded data on the lowest observed vibrational level $v_\Delta=3$. Typically, the intensities of PROBE lines observed following collisional transfer from the predominantly singlet level of the mutually perturbing pair to the predominantly triplet level were $\sim 35\%–40\%$ as strong as the direct double resonance signals through the predominantly singlet level at a buffer gas pressure of ~ 1 Torr.

This strong collisional transfer between mutually perturbing levels of the $A(2)^1\Sigma^+$ and $b(1)^3\Pi$ states appears to be an example of the “gateway effect” first suggested by Gelbart and Freed.¹¹⁸ According to this model, the collision cross section is much greater for transfer of population between the mutually perturbing levels of the two electronic states, than for transfer between nonperturbing levels. Thus, if the $A(2)^1\Sigma^+(v_A, J) \sim b(1)^3\Pi(v_b, J)$ perturbation is strongest for $J=J_p$, the collisional transfer of population from $A(2)^1\Sigma^+(v_A, J_A)$ to $b(1)^3\Pi(v_b, J_b)$ is most likely to occur through a series of collisions utilizing the J_p perturbations as a “gateway:”



where M represents some collision partner, and the transfer from J_A to J_p and from J_p to J_b may occur in one or several steps.

The gateway effect has been observed previously in the homonuclear alkali diatomic molecules Na₂ and Li₂.^{47,119–121} It appears likely that a similar phenomenon is occurring here in the NaK molecule. However, more data is needed to characterize the effect in this case, and this work is planned for the near future.

IV. CONCLUSIONS

We have characterized the NaK $1^3\Delta$ state by the perturbation-facilitated optical–optical double resonance method. Levels of the $1^3\Delta$ state were easily identified by the characteristic intensity pattern of their rotational lines observed in excitation. These patterns are the result of fine and hyperfine structure involving the interaction of the electron and nuclear spins with the other angular momentum vectors in the molecule. From the line positions, we have fit a complete set of Dunham coefficients for the $1^3\Delta$ state and have constructed an RKR potential curve from the experimental data. As has been the case with other electronic states of the NaK molecule that have been studied experimentally,^{28,32,35,36,44,82,88,100,105–109} this experimental potential curve is in excellent agreement with the recent theoretical potentials of Magnier and Millié.⁸⁴

The $1^3\Delta$ state lies between the Hund's case a and Hund's case b coupling limits, but is much closer to case b. The three J levels within an N manifold, $J=N-1$, $J=N$, and $J=N+1$, are split by the spin–orbit interaction in this case. We have studied this fine structure using the deperturbation program, LSQ.⁸⁵ This analysis has resulted in the determination of the spin–orbit interaction constant, which varies slowly with the $1^3\Delta$ state vibrational level. We have also made a relatively crude, first attempt to analyze the $1^3\Delta$ state hyperfine structure. Like most other states of alkali diatomic molecules that have been studied to date, the hyperfine interaction of the NaK $1^3\Delta$ state is dominated by the Fermi contact interaction. In the present case, the $1^3\Delta$ state dissociates to the Na($3S_{1/2}$) + K($3D_{5/2}$) dissociation limit, so the dominant effect is due to the Fermi contact interaction of the electron spin magnetic dipole moment with the sodium nuclear spin moment. We have determined the value of the Fermi contact interaction constant, but additional work should be carried out to refine this value. Ultimately, a complete deperturbation of the combined fine and hyperfine interactions, also taking into account the spin–spin and spin–rotation interactions should be carried out.

Our results indicate that the collisional “gateway” effect, previously observed in Na₂ and Li₂^{47,119–121} is also operating effectively in the NaK $b(1^3\Pi(v_b, J) \sim A(2)^1\Sigma^+(v_A, J)$ system. Further studies to quantify this effect are planned for the near future in our lab.

ACKNOWLEDGMENTS

The authors would like to thank Dr. A. Marjatta Lyyra, Dr. Guenadiy Lazarov, Dr. Mingguang Li, Dr. Yaoming Liu,

Dr. Alan Streater, and Dr. A. Peet Hickman for many valuable discussions on this topic. We would also like to thank Dr. Robert W. Field and Dr. Robert LeRoy for providing computer programs used in this analysis. Laurie Sibbach and Elizabeth Galle were supported through the National Science Foundation Research Experiences for Undergraduates (REU) program.

- ¹R. A. Bernheim, L. P. Gold, and T. Tipton, *J. Chem. Phys.* **78**, 3635 (1983).
- ²S. B. Rai, B. Hemmerling, and W. Demtröder, *Chem. Phys.* **97**, 127 (1985).
- ³R. A. Bernheim, L. P. Gold, C. A. Tomczyk, and C. R. Vidal, *J. Chem. Phys.* **87**, 861 (1987).
- ⁴M. Schwarz, R. Duchowicz, W. Demtröder, and Ch. Jungen, *J. Chem. Phys.* **89**, 5460 (1988).
- ⁵D. A. Miller, L. P. Gold, P. D. Tripodi, and R. A. Bernheim, *J. Chem. Phys.* **92**, 5822 (1990).
- ⁶C. Linton, R. Bacis, P. Crozet, F. Martin, and A. J. Ross, *J. Mol. Spectrosc.* **151**, 159 (1992).
- ⁷C. Linton, F. Martin, P. Crozet, A. J. Ross, and R. Bacis, *J. Mol. Spectrosc.* **158**, 445 (1993).
- ⁸I. Russier, F. Martin, C. Linton, P. Crozet, A. J. Ross, R. Bacis, and S. Churassy, *J. Mol. Spectrosc.* **168**, 39 (1994).
- ⁹K. Urbanski, S. Antonova, A. M. Lyyra, Li Li, and B. Ji, *J. Chem. Phys.* **109**, 912 (1998).
- ¹⁰N. W. Carlson, F. V. Kowalski, R. E. Teets, and A. L. Schawlow, *Opt. Commun.* **29**, 302 (1979).
- ¹¹G. Gerber and R. Möller, *Chem. Phys. Lett.* **113**, 546 (1985).
- ¹²G.-Y. Yan, B. W. Sterling, and A. L. Schawlow, *J. Opt. Soc. Am. B* **5**, 2305 (1988).
- ¹³T.-J. Whang, H. Wang, A. M. Lyyra, Li Li, and W. C. Stwalley, *J. Mol. Spectrosc.* **145**, 112 (1991).
- ¹⁴H. Wang, T.-J. Whang, A. M. Lyyra, Li Li, and W. C. Stwalley, *J. Chem. Phys.* **94**, 4756 (1991).
- ¹⁵Pan Yong-Le, Ma Long-Sheng, Ding Liang-En, and Sun Dian-Ping, *J. Mol. Spectrosc.* **162**, 178 (1993).
- ¹⁶C.-C. Tsai, J. T. Bahns, T.-J. Whang, H. Wang, and W. C. Stwalley, *Phys. Rev. Lett.* **71**, 1152 (1993).
- ¹⁷C.-C. Tsai, J. T. Bahns, and W. C. Stwalley, *J. Chem. Phys.* **99**, 7417 (1993).
- ¹⁸X. Dai, H. Chen, Y. Liu, J. Li, J. Xiang, D. Chen, Li Li, and G.-H. Jeung, *J. Mol. Spectrosc.* **198**, 239 (1999).
- ¹⁹X. Dai, J. Xiang, Y. Liu, and Li Li, *J. Mol. Spectrosc.* **198**, 244 (1999).
- ²⁰A. Katern, P. Kowalczyk, and F. Engelke, *Chem. Phys. Lett.* **146**, 325 (1988).
- ²¹Zhang Kaichang, Qin Lijuan, Wang Zugeng, and Zheng Yishan, *Chin. Phys. Lasers* **15**, 345 (1988).
- ²²H. Wang, Li Li, A. M. Lyyra, and W. C. Stwalley, *J. Mol. Spectrosc.* **137**, 304 (1989).
- ²³Li Li, A. M. Lyyra, H. Wang, and W. C. Stwalley, *Chem. Phys. Lett.* **179**, 417 (1991).
- ²⁴G. Jong, H. Wang, C.-C. Tsai, W. C. Stwalley, and A. M. Lyyra, *J. Mol. Spectrosc.* **154**, 324 (1992).
- ²⁵J. T. Kim, H. Wang, J. T. Bahns, and W. C. Stwalley, *J. Chem. Phys.* **102**, 6966 (1995).
- ²⁶J. T. Kim, C. C. Tsai, and W. C. Stwalley, *J. Mol. Spectrosc.* **171**, 200 (1995).
- ²⁷G. Zhao, J. T. Kim, J. T. Bahns, and W. C. Stwalley, *J. Mol. Spectrosc.* **184**, 209 (1997).
- ²⁸S. Kasahara, M. Baba, and H. Katô, *J. Chem. Phys.* **94**, 7713 (1991).
- ²⁹S. Kasahara, M. Shibata, M. Baba, and H. Katô, *J. Phys. Chem.* **101**, 422 (1997).
- ³⁰S. Kasahara, H. Ikoma, and H. Katô, *J. Chem. Phys.* **100**, 63 (1994).
- ³¹Z. J. Jabbour, Ph.D. thesis, Lehigh University, 1994 (unpublished).
- ³²Z. J. Jabbour and J. Huennekens, *J. Chem. Phys.* **107**, 1094 (1997).
- ³³H. Ikoma, S. Kasahara, and H. Katô, *Mol. Phys.* **85**, 799 (1995).
- ³⁴L.-E. Berg, M. Beutter, and T. Hanson, *Chem. Phys. Lett.* **253**, 327 (1996).
- ³⁵A. Pashov, I. Jackowska, W. Jastrzebski, and P. Kowalczyk, *Phys. Rev. A* **58**, 1048 (1998).
- ³⁶E. Laub, I. Mazsa, S. C. Webb, J. La Civita, I. Prodan, Z. J. Jabbour, R. K. Namiotka, and J. Huennekens, *J. Mol. Spectrosc.* **193**, 376 (1999).

- ³⁷L. M. Andersson, H. O. Karlsson, O. Goscinski, L.-E. Berg, M. Beutter, and T. Hanson, *Chem. Phys.* **241**, 43 (1999).
- ³⁸T. Hansson, *J. Phys. B* **32**, 1997 (1999).
- ³⁹U. Diemer, H. Weickenmeier, M. Wahl, and W. Demtröder, *Chem. Phys. Lett.* **104**, 489 (1984).
- ⁴⁰S. Kasahara, T. Ebi, M. Tanimura, H. Ikoma, K. Matsubara, M. Baba, and H. Katô, *J. Chem. Phys.* **105**, 1341 (1996).
- ⁴¹N. Okada, S. Kasahara, T. Ebi, M. Baba, and H. Katô, *J. Chem. Phys.* **105**, 3458 (1996).
- ⁴²S. Kasahara, C. Fujiwara, N. Okada, H. Katô, and M. Baba, *J. Chem. Phys.* **111**, 8857 (1999).
- ⁴³V. S. Ivanov, V. B. Sovkov, Li Li, A. M. Lyyra, G. Lazarov, and J. Huennekens, *J. Mol. Spectrosc.* **194**, 147 (1999).
- ⁴⁴H. Katô, M. Sakano, N. Yoshie, M. Baba, and K. Ishikawa, *J. Chem. Phys.* **93**, 2228 (1990).
- ⁴⁵Y. Liu, J. Li, H. Gao, D. Chen, Li Li, R. W. Field, and A. M. Lyyra, *J. Chem. Phys.* **108**, 2269 (1998).
- ⁴⁶J. Li, Y. Liu, H. Chen, H. Gao, J. Xiang, D. Chen, G. Wu, Li Li, and R. W. Field, *J. Chem. Phys.* **108**, 7707 (1998).
- ⁴⁷Li Li and A. M. Lyyra, *Spectrochim. Acta A* **55**, 2147 (1999).
- ⁴⁸R. Bombach, B. Hemmerling, and W. Demtröder, *Chem. Phys.* **121**, 439 (1988).
- ⁴⁹L. S. Ma, Y. L. Pan, L. E. Ding, and C. N. Jiang, *Chem. Phys. Lett.* **187**, 116 (1991).
- ⁵⁰Li Li, Q. Zhu, A. M. Lyyra, T.-J. Whang, W. C. Stwalley, R. W. Field, and M. H. Alexander, *J. Chem. Phys.* **98**, 8406 (1993).
- ⁵¹Li Li, Q. Zhu, A. M. Lyyra, T.-J. Whang, W. C. Stwalley, R. W. Field, and M. H. Alexander, *J. Chem. Phys.* **98**, 8413 (1993).
- ⁵²X. L. Chen, H. M. Chen, J. Li, Y. M. Liu, X. C. Dai, G. H. Sha, J. C. Xie, C. H. Zhang, and Li Li, *Chem. Phys. Lett.* **318**, 107 (2000).
- ⁵³X. Xie and R. W. Field, *J. Mol. Spectrosc.* **117**, 228 (1986).
- ⁵⁴Li Li, T. An, T.-J. Whang, A. M. Lyyra, W. C. Stwalley, R. W. Field, and R. A. Bernheim, *J. Chem. Phys.* **96**, 3342 (1992).
- ⁵⁵Li Li, A. Yiannopoulou, K. Urbanski, A. M. Lyyra, B. Ji, W. C. Stwalley, and T. An, *J. Chem. Phys.* **105**, 6192 (1996); **106**, 8626 (1997).
- ⁵⁶D. S. Chen, L. Li, X. T. Wang, Li Li, Q. Hui, H. Ma, L. Q. Li, X. Y. Xu, and D. Y. Chen, *J. Mol. Spectrosc.* **161**, 7 (1993).
- ⁵⁷A. Yiannopoulou, B. Ji, Li Li, M. Li, K. Urbanski, A. M. Lyyra, W. C. Stwalley, and G.-H. Jeung, *J. Chem. Phys.* **101**, 3581 (1994).
- ⁵⁸A. Yiannopoulou, K. Urbanski, A. M. Lyyra, Li Li, B. Ji, J. T. Bahns, and W. C. Stwalley, *J. Chem. Phys.* **102**, 3024 (1995).
- ⁵⁹C. Linton, F. Martin, A. J. Ross, I. Russier, P. Crozet, A. Yiannopoulou, Li Li, and A. M. Lyyra, *J. Mol. Spectrosc.* **196**, 20 (1999).
- ⁶⁰X. Dai, J. O. Clevenger, Y. Liu, M. Song, J. Shang, D. Chen, R. W. Field, and Li Li, *J. Mol. Spectrosc.* **200**, 120 (2000).
- ⁶¹Li Li and R. W. Field, *J. Phys. Chem.* **87**, 3020 (1983).
- ⁶²Li Li and R. W. Field, *J. Mol. Spectrosc.* **123**, 237 (1987).
- ⁶³Li Li, Q. Zhu, and R. W. Field, *J. Mol. Spectrosc.* **134**, 50 (1989).
- ⁶⁴Li Li, Q. Zhu, and R. W. Field, *Mol. Phys.* **66**, 685 (1989).
- ⁶⁵T.-J. Whang, A. M. Lyyra, W. C. Stwalley, and Li Li, *J. Mol. Spectrosc.* **149**, 505 (1991).
- ⁶⁶T.-J. Whang, W. C. Stwalley, Li Li, and A. M. Lyyra, *J. Mol. Spectrosc.* **155**, 184 (1992).
- ⁶⁷G. Lazarov, A. M. Lyyra, Li Li, and J. Huennekens, *J. Mol. Spectrosc.* **196**, 259 (1999).
- ⁶⁸B. Ji, C.-C. Tsai, Li Li, T.-J. Whang, A. M. Lyyra, H. Wang, J. T. Bahns, W. C. Stwalley, and R. J. LeRoy, *J. Chem. Phys.* **103**, 7240 (1995).
- ⁶⁹Y. Liu, J. Li, M. Xue, D. Chen, Li Li, and G.-H. Jeung, *J. Chem. Phys.* **103**, 7213 (1995).
- ⁷⁰J. Li, Y. Liu, H. Gao, M. Xue, D. Chen, and Li Li, *J. Mol. Spectrosc.* **175**, 13 (1996).
- ⁷¹Li Li, A. M. Lyyra, W. T. Luh, and W. C. Stwalley, *J. Chem. Phys.* **93**, 8452 (1990).
- ⁷²J. T. Kim, H. Wang, C.-C. Tsai, J. T. Bahns, W. C. Stwalley, G. Jong, and A. M. Lyyra, *J. Chem. Phys.* **102**, 6646 (1995); **103**, 9891 (1995).
- ⁷³M. Baba, K. Nishizawa, N. Yoshie, K. Ishikawa, and H. Katô, *J. Chem. Phys.* **96**, 955 (1992).
- ⁷⁴K. Ishikawa, *J. Chem. Phys.* **98**, 1916 (1993).
- ⁷⁵K. Ishikawa, N. Mukai, and M. Tanimura, *J. Chem. Phys.* **101**, 876 (1994).
- ⁷⁶H. Katô, M. Otani, and M. Baba, *J. Chem. Phys.* **89**, 653 (1988).
- ⁷⁷Wang Yinde, Wang Chongye, Li Mingguang, and Li Li, *Chinese Phys.-Lasers* **15**, 359 (1988).
- ⁷⁸H. Katô, M. Otani, and M. Baba, *J. Chem. Phys.* **91**, 5124 (1989).
- ⁷⁹H. R. Xia, L. S. Ma, J. W. Xu, M. Yuan, and I. S. Cheng, *Opt. Commun.* **76**, 345 (1990).
- ⁸⁰Y.-C. Wang, K. Matsubara, and H. Katô, *J. Chem. Phys.* **97**, 811 (1992).
- ⁸¹P. Kowalczyk, B. Krüger, and F. Engelke, *Chem. Phys. Lett.* **147**, 301 (1988).
- ⁸²P. Kowalczyk, *J. Chem. Phys.* **91**, 2779 (1989).
- ⁸³K. Ishikawa, T. Kumauchi, M. Baba, and H. Katô, *J. Chem. Phys.* **96**, 6423 (1992).
- ⁸⁴S. Magnier and Ph. Millié, *Phys. Rev. A* **54**, 204 (1996).
- ⁸⁵R. A. Gottscho, J. B. Koffend, and R. W. Field, *J. Mol. Spectrosc.* **82**, 310 (1980).
- ⁸⁶C. R. Vidal and J. Cooper, *J. Appl. Phys.* **40**, 3370 (1969).
- ⁸⁷S. Gerstenkorn and P. Luc, "Atlas du spectre d'absorption de la molécule d'iode," Center National de la Recherche Scientifique, Paris, 1978.
- ⁸⁸A. J. Ross, R. M. Clements, and R. F. Barrow, *J. Mol. Spectrosc.* **127**, 546 (1988).
- ⁸⁹A. J. Ross, C. Effantin, J. d'Incan, and R. F. Barrow, *J. Phys. B* **19**, 1449 (1986).
- ⁹⁰H. Sun, Ph.D. thesis, Lehigh University, 1992 (unpublished).
- ⁹¹H. Sun and J. Huennekens, *J. Chem. Phys.* **97**, 4714 (1992).
- ⁹²G. Herzberg, *Molecular Spectra and Molecular Structure I. Spectra of Diatomic Molecules* (Krieger, Malabar, 1989).
- ⁹³R. N. Zare, *Angular Momentum* (Wiley, New York, 1988).
- ⁹⁴P. F. Bernath, *Spectra of Atoms and Molecules* (Oxford University Press, New York, 1995).
- ⁹⁵H. Lefebvre-Brion and R. W. Field, *Perturbations in the Spectra of Diatomic Molecules* (Academic, Orlando, FL, 1986).
- ⁹⁶C. H. Townes and A. L. Schawlow, *Microwave Spectroscopy* (McGraw-Hill, New York, 1955).
- ⁹⁷K. M. Sando, computer program "DUNHAM," University of Iowa, Department of Chemistry, unpublished.
- ⁹⁸R. J. LeRoy, "DSParFit: Least-squares data fitting program," University of Waterloo, Department of Chemistry, unpublished; "Improved parameterization for diatom Born-Oppenheimer breakdown effects, and a new combined-isotopes analysis for HF and DF," University of Waterloo, Chemical Physics Research Report No. CP-633, 1998.
- ⁹⁹S. Magnier, M. Aubert-Frécon, and Ph. Millié, *J. Mol. Spectrosc.* **200**, 96 (2000).
- ¹⁰⁰A. J. Ross, C. Effantin, J. d'Incan, and R. F. Barrow, *Mol. Phys.* **56**, 903 (1985).
- ¹⁰¹C. E. Moore, "Atomic energy levels," National Bureau of Standards Circular 467, U.S. Government Printing Office, Washington, DC, 1949, Vol. 1.
- ¹⁰²K. M. Sando, computer program "RKR," University of Iowa, Department of Chemistry, unpublished.
- ¹⁰³R. J. LeRoy, "RKR1: A computer program implementing the first-order RKR method for determining diatom potential energy curves from spectroscopic constants," University of Waterloo, Chemical Physics Research Report No. CP-425, 1992.
- ¹⁰⁴See EPAPS Document No. E-JCPSA6-113-001040 for 2 tables (EPAPS Table 1 and EPAPS Table 2). This document may be retrieved via the EPAPS homepage (<http://www.aip.org/pubservs/epaps.html>) or from <ftp.aip.org> in the directory /epaps/. See the EPAPS homepage for more information.
- ¹⁰⁵P. Kowalczyk, W. Jastrzebski, A. Pashov, S. Magnier, and M. Aubert-Frécon, *Chem. Phys. Lett.* **314**, 47 (1999).
- ¹⁰⁶R. F. Barrow, R. M. Clements, G. Delacrézay, C. Effantin, J. d'Incan, A. J. Ross, J. Vergès, and L. Wöste, *J. Phys. B* **20**, 3047 (1987).
- ¹⁰⁷J. Derouard and N. Sadeghi, *J. Chem. Phys.* **88**, 2891 (1988).
- ¹⁰⁸M. Baba, S. Tanaka, and H. Katô, *J. Chem. Phys.* **89**, 7049 (1988).
- ¹⁰⁹P. Kowalczyk, *J. Mol. Spectrosc.* **136**, 1 (1989).
- ¹¹⁰R. J. LeRoy, "LEVEL 6.0: A computer program solving the radial Schrödinger equation for bound and quasibound levels, and calculating various expectation values and matrix elements," University of Waterloo, Chemical Physics Research Report No. CP-555, 1995.
- ¹¹¹I. Kovacs, *Rotational Structure in the Spectra of Diatomic Molecules* (American Elsevier, New York, 1969).
- ¹¹²Li Li, A. M. Lyyra, W. C. Stwalley, M. Li, and R. W. Field, *J. Mol. Spectrosc.* **147**, 215 (1991).
- ¹¹³S. D. Rosner, R. A. Holt, and T. D. Gaily, *Phys. Rev. Lett.* **35**, 785 (1975).
- ¹¹⁴H. Geisen, D. Neuschäfer, and Ch. Ottinger, *Z. Phys. D: At., Mol. Clusters* **4**, 263 (1987).

- ¹¹⁵J. B. Atkinson, J. Becker, and W. Demtröder, *Chem. Phys. Lett.* **87**, 128 (1982).
- ¹¹⁶R. A. Frosch and H. M. Foley, *Phys. Rev.* **88**, 1337 (1952).
- ¹¹⁷H. Katô, *Bull. Chem. Soc. Jpn.* **66**, 3203 (1993).
- ¹¹⁸J. M. Gelbart and K. F. Freed, *Chem. Phys. Lett.* **18**, 470 (1973).
- ¹¹⁹Li Li, Q. Zhu, A. M. Lyyra, T.-J. Whang, W. C. Stwalley, R. W. Field, and M. H. Alexander, *J. Chem. Phys.* **97**, 8835 (1992).
- ¹²⁰Li Li, S. Antonova, A. Yiannopoulou, K. Urbanski, and A. M. Lyyra, *J. Chem. Phys.* **105**, 9859 (1996).
- ¹²¹H. Hulsman and J. Klavins, *Chem. Phys. Lett.* **274**, 85 (1997).